

Vibration-based bearing fault diagnosis using relevant multi-domain features and hierarchical stochastic classification

Diagnóstico de fallos en rodamientos con base en vibraciones empleando características relevantes multi-dominio y clasificación jerárquica estocástica

M. Holguín-Londoño ; G. A. Holguín-Londoño ; C. A. Ramírez-Vanegas 

DOI: <https://DOI.org/10.22517/23447214.24593>

Artículo de investigación científica y tecnológica

Abstract— Bearings installed in industrial electric motors, currently are constituted as the main mode of a failure affecting the global energy consumption. Since energy demand from light industry only grows, demand for effective maintenance in electric motors is critical. Proper life management of such assets focuses on the study of the useful life, delivering efficient information about location and severity of different health status, and using vibration signals from bearings with analysis approaches based on characteristics in time, frequency and time-frequency domains. These domains are characterized by its own benefits as well as its shortcomings, and thus most current works focus only on one of these analyses' domain. This paper studies a possible sub-relevant set of features that favor separability between classes of severity levels to perform training on a concatenation of hierarchical HMM in order to analyze multiple health conditions in bearings, including faults and severities in the following rolling elements: ball, inner race, and outer race. As a result, a substantial improvement is observed in the diagnosis of fault type and severity level present in the bearings and being in concordance with previous studies where just overall process is reported.

Index Terms— Degradation levels, Hierarchical Hidden Markov Models, mode failures, multi-domain analysis, useful life, vibration signals.

Resumen— Los rodamientos instalados en los motores eléctricos industriales, son actualmente la fuente principal de modos de fallos que afectan el consumo energético mundial. Debido a que la demanda energética de la denominada industria ligera solo crece, es crítica la exigencia por mantenimiento efectivo en motores. Una administración adecuada del ciclo de vida de estos activos debe enfrentar el estudio de la vida útil, entregando información eficiente sobre locación y severidad de los diferentes estados de salud, y usando señales de vibración desde los rodamientos con análisis enfocados en características de los dominios del tiempo, la frecuencia y del tiempo-frecuencia. Estos dominios se caracterizan por sus propios beneficios, así como por sus deficiencias, siendo así

que la mayoría de los estudios actuales se enfocan solo en uno de estos dominios de análisis. Este documento estudia un posible conjunto sub-relevante de características que favorezca la separabilidad entre clases y severidades para luego realizar entrenamiento sobre una concatenación de HMM Jerarquizados y con el propósito de analizar múltiples condiciones de salud en rodamientos, incluyendo fallas y severidades en los siguientes elementos rodantes: bola, cara interna y cara externa. Como resultado, se observa una sustancial mejora en el diagnóstico de tipos de fallo y niveles de severidad presentes en rodamientos, y en concordancia con resultados de estudios previos donde no se reportan datos específicos para niveles de severidad.

Palabras claves— Análisis multi-dominio, modelos Ocultos de Markov Jerárquicos, modos de fallos, niveles de degradación, señales de vibración, útil remanente.

I. INTRODUCTION

ROLLER bearings are widely used in industry fields, where reliability has always been paramount [1]. The production of goods that will be sold to the final consumer, like manufacturing of clothes, shoes, furniture, electronics, construction of buildings, automobiles, innovative new energy industries, and in general all produced that is not sold to another manufacturer (also light industry), will experience an incredible 44% growth in energy demand, from a 440 Mtoe in 2018 to an estimated 635 Mtoe for 2040 [2].

Due to operation in difficult conditions, bearing failures often occur, which can have catastrophic consequences. These failures result in dynamic behavior that generates non-stationary vibration signals [1, 3]. And so it is that bearing failures will lead to wind turbine cannot operate properly. The proper management of its maintenance have helped to save up to \$1677 millions per year just in wind energy industry [4, 5]. Therefore, considering the irreplaceable role of the bearing in

Germán Andrés Holguín-Londoño, is with the Electrical Engineering Program, Universidad Tecnológica de Pereira, Pereira, Colombia (e-mail: gahol@utp.edu.co)

Carlos Alberto Ramírez-Vanegas, is with the Mathematics Department, Universidad Tecnológica de Pereira, Pereira, Colombia (e-mail: caramirez@utp.edu.co)

This manuscript was sent on October 28, 2020 and accepted on June 30, 2021. This work was supported by “Diseño y desarrollo de un sistema prototipo en línea para el diagnóstico de motores de combustión interna diésel en servicio con base en vibraciones mecánicas. Aplicación a los sistemas de transporte masivo,” funded by MinCiencias (Colciencias) Cod. 1110-669-46074.

Mauricio Holguín-Londoño, is with the Electrical Engineering Program, Universidad Tecnológica de Pereira, Pereira, Colombia (e-mail: mau.hol@utp.edu.co)



the operation process, it is very important to monitor and predict its health status [6, 7].

Currently, research focuses on the Useful Life, since it allows for managing the residual risk in equipment before it fails [8]. In such scenario, diagnosis is a classification problem while prognosis must deliver results on location and severity (the result of a failure mode in the system function perceived by the user), following a process of detection of occurrence and perform statistical analysis of the observed characteristics in order to reach a decision in the state of structural health.

Vibration signals from the bearings are quasi-stationary in nature, with varying parameters over time holding nonstationary noisy and nonlinear characteristics. Due to the system nature, these parameters will vary even when signals come from supposedly identical equipment [9]. Current strategies based on signal analysis look for features in time, frequency, and time-frequency domains [10]. In the time domain, features are mainly based on the statistical behavior of the waveform, but do not adequately reflect the change in frequency components as the progression of a fault develops [11]. In the frequency domain, traditional techniques include the Fast Fourier Transform (FFT) and power spectrum, but given the nature of the signals, these analyses can be insensitive to changes in time of the intensity of frequency components [10]. Other strategies use techniques in the time-frequency domain, such as Wavelets, which are notorious for being sensitive to the selection of tuning parameters [12]. Furthermore, the analysis of extracted features usually falls on a single domain, namely time, frequency or time-frequency [10]. However, these studies are not considering the contribution of each of these domains to the discrimination of the degradation process. Described approaches also lack the combination of domains [13].

The Hidden Markov Models (HMM) are suitable for the analysis of random dynamical systems, in order to make predictions about the diagnosis of the degradation process [14]. However, when the number of failure modes grows, HMMs require a large number of training states. One variant of the HMM is the Hierarchical Hidden Markov Models (HHMM), which behave as a chain of sub-hierarchical HMM analyzing multiple health states. It is important to note that the accuracy of a diagnostic system involving various types of faults and levels of severity should be evaluated considering the accuracy and variability in each class [13].

In this work, we introduce a signal-based approach to support bearing diagnosis by fault type and severity evaluation. Furthermore, we present an analysis of extracted features from vibration signals in bearings using time, frequency, and time-frequency domains in order to determine the smallest set of feature combinations for each level in an HHMM framework. The rest of the paper is organized as follows: a brief review about multi-domain feature extraction, HMM, and HHMM, it is presented in the theoretical background section; the data base and the experimental framework definition is shown in the experimental setup section; experimental validation and observation are illustrated in the results and the discussion section; finally, the conclusions and the acknowledgments are

given.

II. THEORETICAL BACKGROUND

A. Multi-domain feature extraction

For discriminating bearing faults from vibration signals, three different feature domains are considered: First, the time domain (T) is the natural representation [15]. Here, 17 temporal features are extracted from given signal $\mathbf{z} \in \mathbb{R}^T$, namely: the mean, the standard deviation, the skewness, the kurtosis, the maximum, the root mean square, the shape factor, the unsigned mean factor, the clearance factor, the impulse factor, the upper and lower bound histogram values, the likelihood value, the Shannon's entropy value, the root mean square over signal peaks, and the standard deviation of signal values greater than the 70th percentile. Second, the following 16 frequency-based (F) features are extracted from the FFT representation of \mathbf{z} [15]: the mean, the variance, the skewness, the kurtosis, the center frequency, the standard deviation, the root mean square, the mean square, the inverse root mean square, the standard deviation of frequency values greater than the center frequency, the mean over the skewness, the mean over the kurtosis, the root mean square over the mean, the root of the geometric mean, the mean absolute deviation, and the interquartile range. Finally, some time-frequency-based features are also extracted from the well-known Mel-Frequency Cepstral Coefficients (MFCC) aiming to highlight both linear and nonlinear signal properties [16]. MFCC have two filter types, linearly distributed for frequencies below 1 kHz, and logarithmically distributed for frequencies above 1 kHz. The MFCC implementation involves the following steps: Segmentation for dividing the signal into small frames; Windowing through a Hamming window to adjust the frames and to integrate all the closest frequency lines; Pre-Emphasis, or filtering to emphasize the higher frequencies; Fast Fourier Transform; Mel filters, or the bank of filters with a band pass triangular frequency response; Discrete Cosine Transform to convert the Mel spectrum into time domain; and Delta Energy Spectrum with 13 velocity deltas and 39 double deltas or accelerations, due to the quasi-stationary nature of the signals affecting frames as they overlap in their transition [17]. Thereby, we carry out the MFCC representation with a 24 filter bank and 12 coefficients. Thus, an input multi-domain feature matrix $\mathbf{X} \in \mathbb{R}^{N \times L}$ is built after vector concatenation of T, F, and MFCC measurements, where N and L are the number of samples and features, respectively.

B. Hierarchical Hidden Markov Model

A Markov Model is any system that at certain instant t , belongs to a state from a finite set $\Psi = \{\mathbf{S}_r: r \in \mathbf{1}, \dots, \mathbf{R}\}$. Thus, at discrete uniformly distributed instants, the system performs state transitions according to a set of transition probabilities, for a time t at the current state \mathbf{q}_t . Based on the Markovian property, the transition probability only depends on the previous state $\mathbf{P}\{\mathbf{q}_t = \mathbf{S}_j | \mathbf{q}_{t-1} = \mathbf{S}_j, \mathbf{q}_{t-2} = \mathbf{S}_j, \dots\} = \mathbf{P}\{\mathbf{q}_t = \mathbf{S}_j | \mathbf{q}_{t-1} = \mathbf{S}_j\}$, besides, the output symbols of the different observable states $\Lambda = \{\mathbf{V}_m: m \in \mathbf{1}, \dots, \mathbf{M}\}$ are emitted with

probability distribution at the state j given by $\mathbf{b}_j(\mathbf{m}) = \mathbf{P}\{\mathbf{v}_m \text{ at } t | \mathbf{q}_t = \mathbf{S}_j\}$. Since the output is a probabilistic function of the states, the model comprises a double embedded stochastic process, which is indirectly observable through the set of output sequences (Hidden Markov Model (HMM)) [18].

With the aim of discovering complex data relationships in bearing fault diagnosis tasks, we introduced a Hierarchical Hidden Markov Model (HHMM) applied to the multi-domain feature representation matrix \mathbf{X} . In particular, we propose a hierarchical Markov chain where the higher HMM layer has HMM states as part of their hidden states. In this sense, our HHMM requires fixing the topological structure ζ , the model parameters, and the observations alphabet Σ .

The topological structure ζ determines the hierarchical levels $\mathbf{D} \in \mathbb{N}$ and the number of states $\mathbf{Q} \in \mathbb{N}$ by level $\zeta = \{\forall \mathbf{d}_i : \exists \mathbf{Q}_i^{\mathbf{d}} | \mathbf{d}_i \in \mathbf{1} \dots \mathbf{D}\}$. Note that if the number of states per level is the same, then, the subscript i is omitted in $\mathbf{Q}_i^{\mathbf{d}}$. Now, the model parameters $\boldsymbol{\eta} = \{\mathbf{A}, \mathbf{B}, \boldsymbol{\Pi}\}$ are estimated by the horizontal transition matrix

$$\mathbf{A} = \left\{ \forall \mathbf{A}^{\mathbf{q}_i^{\mathbf{d}}} = \left(\mathbf{a}_{ij}^{\mathbf{q}_i^{\mathbf{d}}} \right) | \mathbf{a}_{ij}^{\mathbf{q}_i^{\mathbf{d}}} = \mathbf{P}(\mathbf{q}_j^{\mathbf{d}+1} | \mathbf{q}_i^{\mathbf{d}+1}) \right\}, \quad \text{the}$$

$$\text{observations probability } \mathbf{B} = \left\{ \forall \mathbf{B}^{\mathbf{q}_i^{\mathbf{d}}} = \left(\mathbf{b}^{\mathbf{q}_i^{\mathbf{d}}}(\mathbf{k}) \right) | \mathbf{b}^{\mathbf{q}_i^{\mathbf{d}}}(\mathbf{k}) = \mathbf{P}(\sigma_{\mathbf{k}} | \mathbf{q}^{\mathbf{d}}), \sigma_{\mathbf{k}} \in \Sigma \right\} \text{ and the vertical transition vector}$$

$$\boldsymbol{\Pi} = \left\{ \forall \boldsymbol{\Pi}^{\mathbf{q}_i^{\mathbf{d}}} = \boldsymbol{\pi}^{\mathbf{q}_i^{\mathbf{d}}}(\mathbf{q}_i^{\mathbf{d}+1}) | \boldsymbol{\pi}^{\mathbf{q}_i^{\mathbf{d}}}(\mathbf{q}_i^{\mathbf{d}+1}) = \mathbf{P}(\mathbf{q}_i^{\mathbf{d}+1} | \mathbf{q}_i^{\mathbf{d}}) \right\}.$$

The horizontal transition matrix informs the transition probabilities between nodes belonging to the same level meanwhile the vertical transition vector encodes the transition probabilities from higher-level nodes to lower-level nodes [19].

III. EXPERIMENTAL SETUP

For all provided experiments, the bearing fault diagnosis database developed by the Bearing Data Center at Case Western Reserve University is employed [20]. Vibration signals were acquired at 12kHz and failures were induced by electro-discharge of 0.0178, 0.0356, and 0.0533 cm in diameter with 0.028 cm depth size. The faults are labeled as L1, L2, and L3 (low, middle, and high levels, respectively) at three different Rolling elements (failure modes), namely: the Ball, the Inner race, and the Outer race, plus the Normal state. The data base is organized in 10 folders, one for each rolling element and each fault label, plus the normal operation. For a folder, there are 12 registers of 3.3 s, to each one a Hamming window is applied to obtain signal segments of 200 ms with $\frac{2}{3}$ overlap. The preceding parameter values are based on data reported by [21]. So, the multi-domain feature matrix has a total of $\mathbf{N} = \mathbf{48}$ signal segments and $\mathbf{L} = \mathbf{45}$ characteristics (17 for T, 16 for F, and 12 for M, respectively).

For each provided segment, the three different representation domain features described previously (Time (T), Frequency (F), and MFCC (M)) are computed. Further, a codebook building stage is performed to build the HHMM states to compute a compact discrete representation from the multi-domain features. Here, the distortion rate is applied to select the number of centroids of the k-means algorithm [22], where a distortion curve of the clustering method is generated for different values of \mathbf{k} . The distortion of a data grouping is defined as: Be a set of

data (\mathbf{X}) modeled by random variables of dimension \mathbf{p} , consisting of a mixture of distributions with common covariance components (\mathbf{S}), and for \mathbf{k} clusters, with centers \mathbf{c}_x as near as possible to a given sample in \mathbf{X} , the minimum average distortion per dimension when fixed the number of centers is given by $\mathbf{d}_k = \frac{1}{\mathbf{p}} \min_{\mathbf{c}_1 \dots \mathbf{c}_k} E[(\mathbf{X} - \mathbf{c}_x)^T \mathbf{S}^{-1} (\mathbf{X} - \mathbf{c}_x)]$.

The jumps in the resulting values mean reasonable selections of \mathbf{k} , with the largest jump representing the best selection. In particular, the change in distortion between the previous and current cluster was analyzed for values from 2 to 30. It was found that out of a total of 10 replicates, 80% of the time the groups ranged from 22 to 25 groups, so $\mathbf{k} = \mathbf{24}$ was selected.

Finally, the HHMM models are trained for a two-layer structure ($\mathbf{D} = \mathbf{2}$) by varying the number of states between 2 and 3 states ($\mathbf{Q} = \mathbf{2}, \mathbf{3}$). The first layer is carried out to identify the type of fault, and the second layer is related to the severity level, as seen in Fig. 1. A cross validation scheme with 30 repetitions is used by randomly selecting 60% of the samples as the training set.

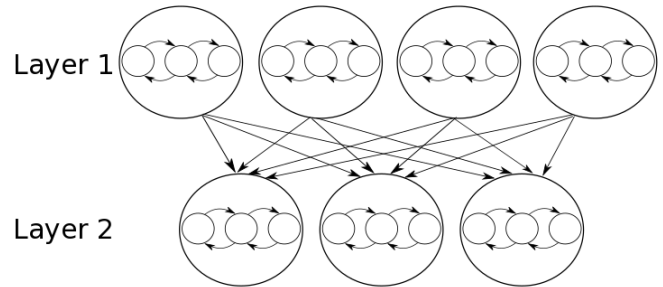


Fig. 1. HHMM representation, were first layer identify the type of fault, and the second layer the severity level. Source: Authors.

IV. RESULTS AND DISCUSSION

A. Feature domain analysis

Our bearing fault diagnosis system is tested as a tool to classify the type of fault. In this case, the first layer of the HHMM-based classification is used. Moreover, the three different features domains are validated aiming to assess their effectiveness. Table I presents the cross-validation results, showing the mean and standard deviation values for the classification performance of the failure types in the set of representation domains indicated by the first column. The number of states value \mathbf{Q} in HHMM is also presented. From Table I, an acceptable type of fault diagnosis performance is achieved for all considered domains. Especially notable is the accuracy for M-domain. Nonetheless, finding a subset of relevant features decreases the data redundancy to favor further classification stages, in fact, the best classification results are obtained for the M-based features. Moreover, diagnosis of the normal state is possible for all domains at this layer, with lower accuracy for the frequency domain.

Now, Table II shows the severity level classification results for each type of fault. Namely, the second layer of HHMM is trained according to the different feature-domain combinations. Again, the number of states Q is presented. Note that the normal operation class does not require a severity level diagnosis. Achieved results show that the severity level classification accuracies are lower than the type of fault ones, which can be explained by the complex data relationships regarding the induced level failures. In particular, discriminating the severity level for the ball fault is a challenging task. However, the M-

TABLE I
FEATURE-DOMAIN ANALYSIS FOR TYPE OF FAULT CLASSIFICATION. SOURCE: AUTHORS

| Domain | Q | Ball | Inner | Normal | Outer |
|--------|-----|--------------------|--------------------|--------------------|--------------------|
| T | 2 | 1.000±0.000 | 0.920±0.121 | 1.000±0.000 | 0.960±0.047 |
| | 3 | 1.000±0.000 | 0.973±0.047 | 1.000±0.000 | 0.960±0.084 |
| F | 2 | 0.987±0.042 | 0.913±0.077 | 0.960±0.084 | 0.980±0.032 |
| | 3 | 1.000±0.000 | 0.940±0.058 | 0.940±0.190 | 0.967±0.065 |
| M | 2 | 0.993±0.021 | 1.000±0.000 | 1.000±0.000 | 1.000±0.000 |
| | 3 | 1.000±0.000 | 1.000±0.000 | 1.000±0.000 | 1.000±0.000 |
| TF | 2 | 1.000±0.000 | 1.000±0.000 | 1.000±0.000 | 0.973±0.047 |
| | 3 | 1.000±0.000 | 0.980±0.032 | 1.000±0.000 | 0.953±0.055 |
| TM | 2 | 1.000±0.000 | 0.960±0.056 | 1.000±0.000 | 0.967±0.035 |
| | 3 | 1.000±0.000 | 0.980±0.063 | 1.000±0.000 | 0.973±0.034 |
| FM | 2 | 1.000±0.000 | 0.947±0.053 | 0.980±0.063 | 0.987±0.042 |
| | 3 | 1.000±0.000 | 0.953±0.063 | 0.980±0.063 | 0.987±0.028 |
| TF M | 2 | 0.993±0.021 | 0.960±0.084 | 0.980±0.063 | 0.953±0.045 |
| | 3 | 1.000±0.000 | 0.967±0.057 | 1.000±0.000 | 0.940±0.066 |

based features allow revealing a suitable representation space that ensures suitable discrimination performances. This layer shows the convenience of a hierarchical based model.

B. Intra-domain feature relevance analysis

In this experiment, we test the intra-domain feature capability for discriminating bearing faults and severities using the

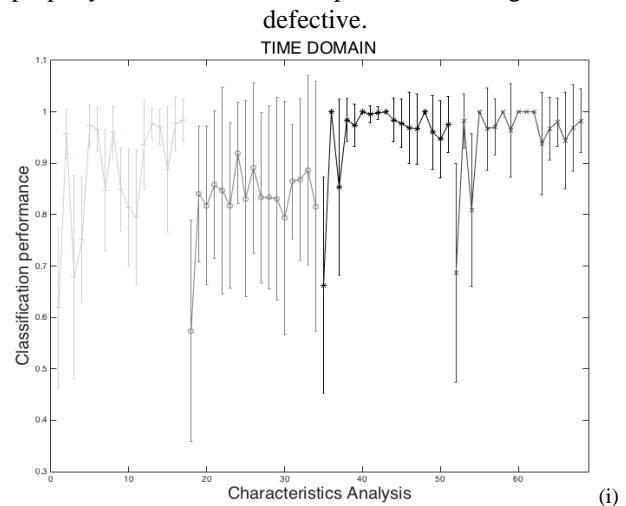
TABLE II
FEATURE-DOMAIN ANALYSIS FOR SEVERITY LEVEL CLASSIFICATION WITHIN EACH BEARING FAULT. SOURCE: AUTHORS

| Domain | Q | Ball | Inner | Outer |
|--------|-----|--------------------|--------------------|--------------------|
| T | 2 | 0.840±0.145 | 1.000±0.000 | 1.000±0.000 |
| | 3 | 0.860±0.093 | 1.000±0.000 | 0.980±0.063 |
| F | 2 | 0.920±0.090 | 1.000±0.000 | 0.980±0.051 |
| | 3 | 0.927±0.111 | 1.000±0.000 | 0.960±0.084 |
| M | 2 | 1.000±0.000 | 1.000±0.000 | 0.960±0.063 |
| | 3 | 0.920±0.051 | 1.000±0.000 | 1.000±0.000 |
| TF | 2 | 0.873±0.125 | 1.000±0.000 | 1.000±0.000 |
| | 3 | 0.827±0.108 | 1.000±0.000 | 1.000±0.000 |
| TM | 2 | 0.867±0.138 | 1.000±0.000 | 0.980±0.063 |
| | 3 | 0.660±0.250 | 1.000±0.000 | 1.000±0.000 |
| FM | 2 | 0.820±0.114 | 1.000±0.000 | 0.973±0.064 |
| | 3 | 0.900±0.144 | 1.000±0.000 | 0.973±0.047 |
| TF M | 2 | 0.893±0.113 | 1.000±0.000 | 1.000±0.000 |
| | 3 | 0.907±0.110 | 1.000±0.000 | 0.980±0.063 |

introduced HHMM. Fig. 2 shows the attained results by analyzing each fault class, where the number of characteristics varies with the domain analyzed, thus: in T (Fig. 2-i) we analyze the 17 characteristics in each class (ball, inner, normal, and outer) for a total of 68; In F (Fig. 2-ii), 16 characteristics are analyzed in each class, for a total of 64; and in M (Fig. 2-iii) we have 12 characteristics in each class, for a total of 48. In Fig. 2 the points according to failure types, or classes, are indicated as follows: Ball (+), Inner (o), Normal (*), Outer (x), and the y-axis is the performance rating value. As seen, frequency domain features show uniform accuracy, meanwhile melcepstrum features evidence variable accuracy. Furthermore, individual features from frequency and melcepstrum domains show the better results at severity level diagnosis.

Afterward, we carry out a forward and backward analysis to highlight feature subsets for each domain. According to Fig. 3 and 4 it is possible to notice how the set of features for each domain present different discrimination capacity between the two layers. In Fig. 3- (i), (ii) and (iii) the x-axis represents the number of characteristics in the forward analyzed subset by class, and in Fig. 4- (i), (ii) and (iii) the x-axis represents the number of characteristics eliminated in the backward analyzed subset by class. In both figures the y-axis is the performance rating value, and the points according to failure types, or classes, are indicated as follows: Ball (+), Inner (o), Normal (*), Outer (x).

Thus, the first layer of the HHMM proposed only considers the features 1, 2, 4, 6, 8, and 9 of the M-domain. With respect to the second layer, the features 2, 3, 9, 12, 13 and 16 of the F-domain are employed to classify the severity level. For the sake of simplicity, the number of states is fixed to two. This results are in concordance with observations reported in others papers, like in [23], where the authors report that with cepstral analysis a fault can be detected and its nature identified with a certain amount of confidence, as well as frequency domain techniques are adequate to identify faults, but does not work properly to determine the component of bearing which is



(i)

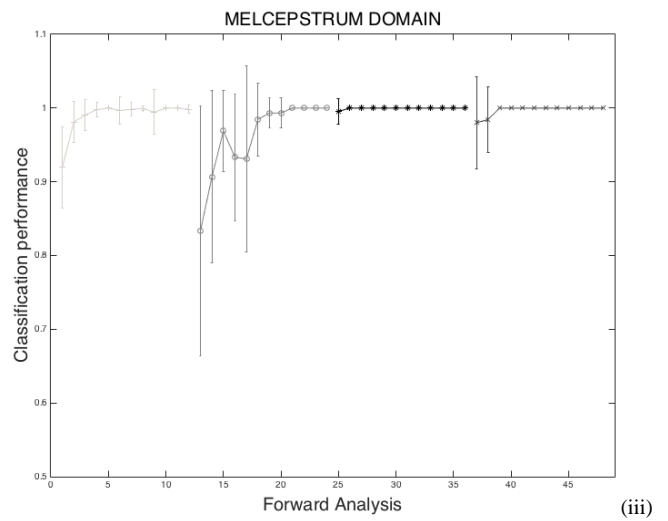
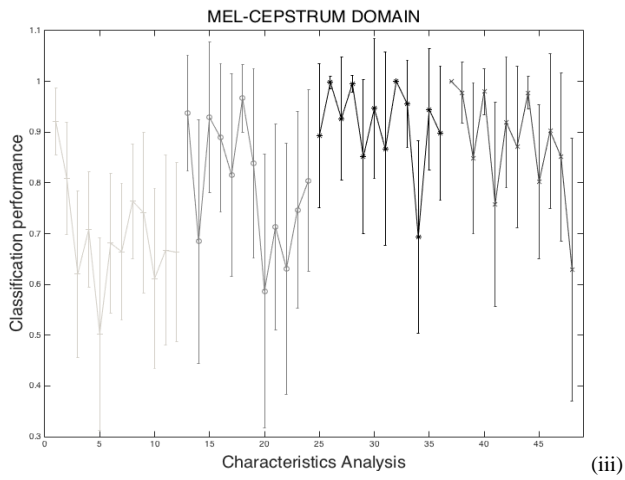
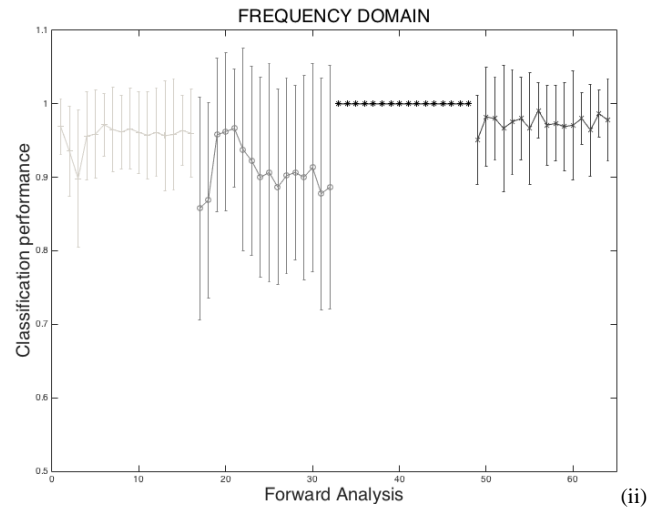
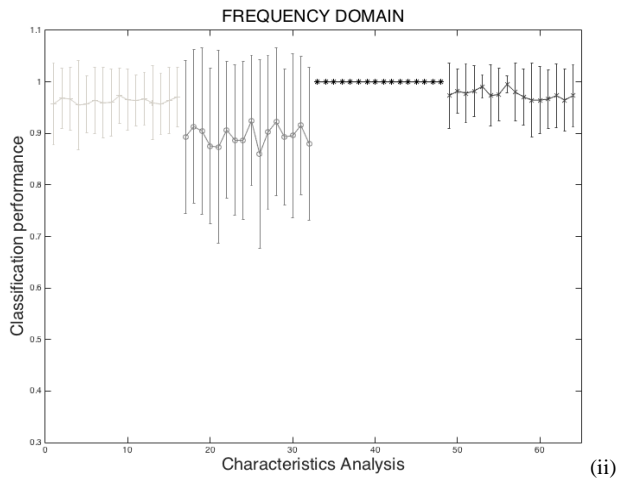
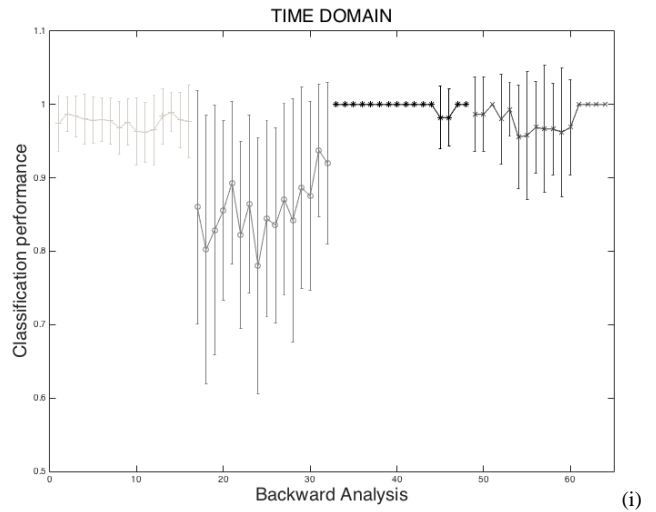
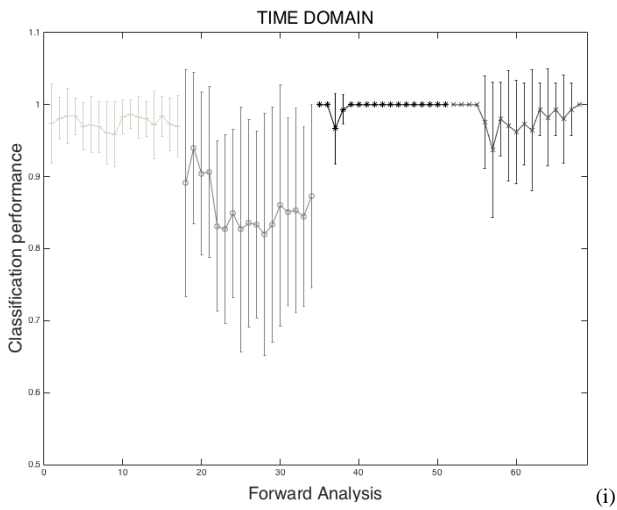


Fig. 2. Feature relevance analysis for type of fault and severity level diagnosis. Severity level classification performance: Ball (+), Inner (o), Normal (*), Outer (x). Source: Authors.

Fig. 3. Forward feature relevance analysis for type of fault and severity. Severity level classification performance: Ball (+), Inner (o), Normal (*), Outer (x). Source: Authors.



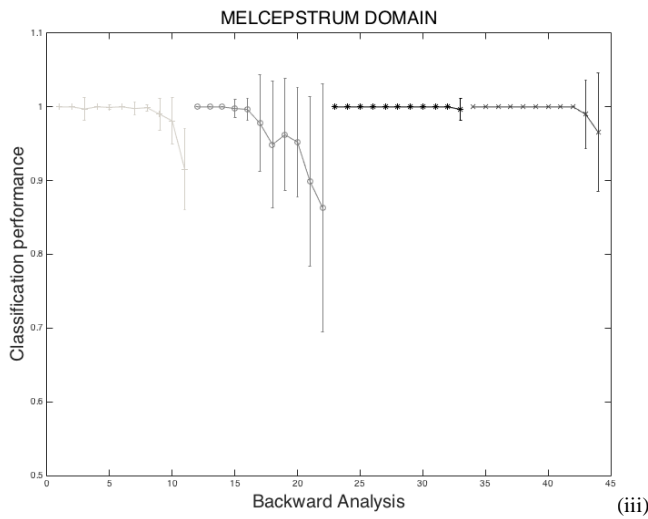
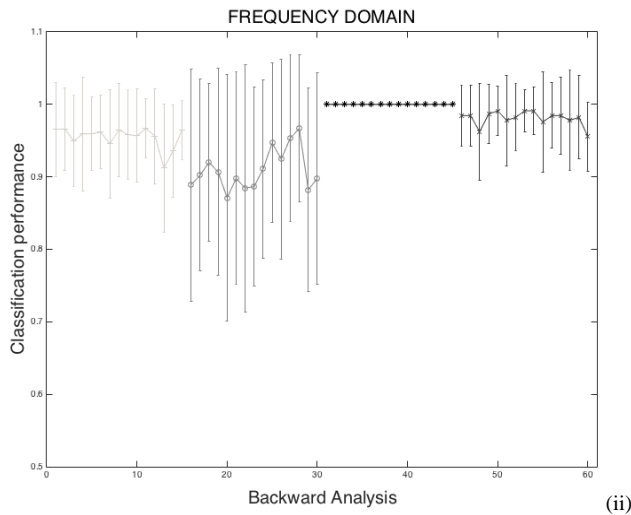


Fig. 4. Backward feature relevance analysis for type of fault and severity. Severity level classification performance: Ball (+), Inner (o), Normal (*), Outer (x). Source: Authors.

Table III presents the bearing fault classification results by applying both HHMM over the relevant feature subset (RF-HHMM) and HHMM over the whole multi-domain feature set (WS-HHMM). As seen, the RF-HHMM preserves the diagnosis performance in comparison to the WS-HHMM. Indeed, the estimated feature set is able to find out relevant patterns for identifying complex classes, e.g., Ball and Outer faults at level L1. The worst classification performance is obtained for Ball fault at level 3 for both studied strategies (0.87 and 0.84). Then, the WS-HHMM and the RF-HHMM mean results (0.975 and 0.981, respectively) demonstrate that bearing fault dynamics can be differentiated from vibration signals if a relevant feature subset is estimated for both fault type and severity level. In addition, since the probability of detection of a failure type is 100% in both schemes, the conditional probability of detecting a severity level is independent of the failure type.

TABLE III

HHMM-BASED BEARING FAULT DIAGNOSIS. WS: WHOLE MULTI-DOMAIN FEATURE SET, RF: RELEVANT FEATURE SET. L1, L2, AND L3 STAND FOR LOW, MIDDLE, AND HIGH SEVERITY LEVEL. SOURCE: AUTHORS.

| Strategy | Layer | Ball | Inner | Outer | Normal | Total |
|-----------|--------------|------------------|------------------|------------------|----------------|--------------|
| WS-HHMM | 1 | 1.00±0.00 | 1.00±0.00 | 1.00±0.00 | | |
| | 2, L1 | 0.91±0.15 | 1.00±0.00 | 0.84±0.26 | 1.0±0.0 | |
| | 2, L2 | 0.99±0.04 | 1.00±0.00 | 1.00±0.00 | | |
| | 2, L3 | 0.87±0.15 | 1.00±0.00 | 1.00±0.00 | | |
| | Total | 0.94±0.11 | 1.00±0.00 | 0.96±0.09 | 1.0±0.0 | 0.975 |
| RF-HHMM | 1 | 1.00±0.00 | 1.00±0.00 | 1.00±0.00 | | |
| | 2, L1 | 0.93±0.15 | 1.00±0.00 | 0.95±0.18 | 1.0±0.0 | |
| | 2, L2 | 0.98±0.06 | 1.00±0.00 | 1.00±0.00 | | |
| | 2, L3 | 0.84±0.17 | 1.00±0.00 | 0.99±0.06 | | |
| | Total | 0.94±0.10 | 1.00±0.00 | 0.99±0.07 | 1.0±0.0 | 0.981 |
| ANFIS[10] | | | | | | 0.970 |

Previous achieved results are in accordance with the approach presented by authors in [10], where a Discrete Wavelet Transform (DWT) and an Adaptive Neural Fuzzy Inference System (ANFIS) approach was proposed to automate the fault detection and diagnosis process, and a mean average classification of 0.97 is reported classifying the same data base. This ANFIS is based on a 5-layer system, where layer 1 implement the fuzzification, layer 2 is a fuzzy AND operation, layer 3 is normalization, layer 4 is fuzzy inference, and finally, layer 5 is a defuzzification layer. Authors in paper [10] do not report results per severity level or fault type, but only for overall process.

V. CONCLUSION

Individually, the characteristics in each representation domain provide diverse variability in the discrimination process in both layers. While the characteristics of F-domain behave uniformly in all layers, in M-domain they show a different behavior between layers. In addition, individually, the characteristics of the F and M domains present better results when detecting levels of severity.

On the other hand, the number of features required in each domain, to obtain diagnostic accuracy comparable to having the entire feature set, can be appreciably reduced. This justifies the need to use several representation domains and reduced sets of characteristics. Furthermore, the proposed two-layer model with different representation domains in each and a reduced set of features, has a diagnostic accuracy comparable to the same model using the full set of features.

According to the results obtained, the time-frequency-based features are the most relevant for separating the type of fault and the frequency-based parameters favor the discriminations between levels of severity. Moreover, achieved results are in accordance with the state of art ones. However, our strategy is able to extract a relevant subset of features which favors further learning stages by coding complex data relationships related to hidden interactions between fault type and severity level.

ACKNOWLEDGMENT

This work was supported by “Diseño y desarrollo de un

sistema prototipo en línea para el diagnóstico de motores de combustión interna diésel en servicio con base en vibraciones mecánicas. Aplicación a los sistemas de transporte masivo,” funded by MinCiencias (Colciencias) Cod. 1110-669-46074. Special acknowledgment to Universidad Tecnológica de Pereira.

REFERENCES

- [1] Ruonan, L., Boyuan, Y., Hauptmann, G. Simultaneous bearing fault recognition and remaining useful life prediction using joint-loss convolutional neural network. *IEEE Transactions on industrial informatics*, vol. 16, No. 1, pp 87-96, January 2020.
- [2] IEA, Change in final energy consumption by sector, 2000-2018, and by scenario to 2040, IEA, Paris <https://www.iea.org/data-and-statistics/charts/change-in-final-energy-consumption-by-sector-2000-2018-and-by-scenario-to-2040>.
- [3] Gougam, F., Rahmoune, C., Benazzouz, D., Varnier, C., Nicod, J-M. Health monitoring approach of bearing: application of adaptive neuro fuzzy inference system (ANFIS) for RUL-estimation and autogram analysis for fault-localization. 2020 Prognostics and Health Management Conference. 2020.
- [4] Xiaohang, J., Zijun, Q., Yi, S. Development of vibration-based health indexes for bearing remaining useful life prediction. *Prognostics & System Health Management Conference—Qingdao*. 2019.
- [5] Jin, X., Que, Z., Sun, Y., Guo, Y., Qiao, W. “A data-driven approach for bearing fault prognostics,” *IEEE Trans. on Ind. Appl.*, vol.55, no. 4, pp. 3394-3401, July/August 2019.
- [6] Jinbing, L., Kai, Z., Min, H., Jun, W. Reconstruction-based fault prognosis for bearings with principal component analysis. *Proceedings of the 38th Chinese Control Conference July 27-30, Guangzhou, China*. 2019.
- [7] Elforjani, M., Shanbr, S. Prognosis of bearing acoustic emission signals using supervised machine learning. *IEEE Trans. on Industrial Electronics*, 65(7), pp. 5864–5871, 2018.
- [8] Sikorska, J., Hodkiewicz, M., Ma, L.: Prognostic modelling options for remaining useful life estimation by industry. *MSSP* 25(5) (2011) 1803 – 1836.
- [9] Janjarasjitt, S., Ocak, H., Loparo, K.: Bearing condition diagnosis and prognosis using applied nonlinear dynamical analysis of machine vibration signal. *Journal of Sound and Vibration* 317(1–2) (2008) 112 – 126.
- [10] Attoui, I., Boutasseta, N., Fergani, N., Oudjani, B., Deliou, A.: Vibration-based bearing fault diagnosis by an integrated dwt-fft approach and an adaptive neuro-fuzzy inference system. In: *CEIT, 2015 3rd International Conference on*. (May 2015) 1–6.
- [11] Jardine, A.K., Lin, D., Banjevic, D.: A review on machinery diagnostics and prognostics implementing condition-based maintenance. *MSSP* 20(7) (2006) 1483 – 1510.
- [12] Darley, S., Robson, P.: Application of wavelet transform to detect faults in rotating machinery. In: *ABCM Symposium Series in Mechatronics*. (2004) 616–624.
- [13] Cococcioni, M., Lazzarini, B., Volpi, S.L.: Robust diagnosis of rolling element bearings based on classification techniques. *IEEE Transactions* 9(4) (Nov 2013) 2256–2263.
- [14] Zaidi, S.S.H., Aviyente, S., Salman, M., Shin, K.K., Strangas, E.G.: Prognosis of gear failures in dc starter motors using hmm. *IEEE Transactions* 58(5) (May 2011) 1695–1706.
- [15] Cardona, O.: Análisis tiempo-frecuencia de señales de vibraciones mecánicas para la detección de fallos en máquinas rotativas. Master’s thesis, *Automatización Industrial*, Universidad Nacional de Colombia, Manizales, Colombia (2011).
- [16] Nelwamondo, F.V., Marwala, T.: Faults detection using gaussian mixture models, melfrequency cepstral coefficients and kurtosis. In: *2006 IEEE International Conference on Systems, Man and Cybernetics*. Volume 1. (Oct 2006) 290–295.
- [17] Muda, L., Begam, M., Elamvazuthi, I.: Voice Recognition Algorithms using Mel Frequency, Cepstral Coefficient (MFCC) and Dynamic Time Warping (DTW) Techniques. *Journal of computing*. Vol. 2, Issue 3. ISSN: 2151-9617. March, 2010.
- [18] Ephraim, Y., Merhav, N.: Hidden markov processes. *IEEE Transactions on Information Theory* 48(6) (Jun 2002) 1518–1569.
- [19] Samko, O., Marshall, A.D., Rosin, P.L.: Automatic construction of hierarchical hidden markov model structure for discovering semantic patterns in motion data. In: *Proceedings of VISIGRAPP 2010*. (2010) 275–280.
- [20] Loparo, K.: Seeded fault test data, bearing data center, case western reserve university. <http://csegroups.case.edu/bearingdatacenter/pages/download-data-file>.
- [21] Castaño, J.C., Agudelo, C.H.: “Extensibilidad de criterios de decisión para un clasificador de fallos en rodamientos basado en HMM, sobre resultados en un clasificador de menos estados, empleando características en diferentes espacios de representación”. Undergraduate thesis. *Electric Engineering*, Universidad Tecnológica de Pereira. T621.31042 C346; 6310000108472 F3256, 2015. URL: <http://hdl.handle.net/11059/5198>.
- [22] Kolesnikov, A., Trichina, E.: Determining the Number of Clusters with Rate-Distortion Curve Modeling. *Image Analysis and Recognition Lecture Notes in Computer Science*, Vol. 7324, pp 43-50, 2012.
- [23] Boudiaf, A., Moussaoui, A., Dahane, A., Atoui, I.: A Comparative Study of Various Methods of Bearing Faults Diagnosis Using the Case Western Reserve University Data. *J Fail. Anal. and Preven.* (2016) 16: 271–284. DOI: 10.1007/s11668-016-0080-7.



Mauricio Holguín-Londoño was born in Pereira, Risaralda, Colombia in 1974. He received the B.S. and M.S. degrees in electrical engineering from the Universidad Tecnológica de Pereira (UTP), Risaralda, in 2009 and the Ph.D. in engineering, automatic area, from the

UTP, Pereira, Risaralda, in 2018. From 2006 to 2008, he was a Research Assistant with the Automatic Research Group in UTP. From 2009 to 2014, he was an Assistant Professor with the Electrical Engineering Program. Since 2014, he has been an Associate Professor with the Engineering Faculty, UTP, Pereira. He is the author of three books, more than 30 articles, and more than 25 software related products. Since 2010, he has been researcher and director of the research group in Management of Electrical, Electronic and Automatic Systems. His research interests include applications in industrial instrumentation, automatic control, quality control, asset management of electrical systems and autonomous maintenance, inspection, reliability and quality control systems with non-invasive techniques.

Dr. Hoguín-Londoño was a recipient of the recognition as a distinguished student of the UTP in 1997.

ORCID:



Germán Andrés Holguín-Londoño was born in Pereira, Colombia in 1977. He received the B.S. and M.S. degrees in electrical engineering from the Universidad Tecnológica de Pereira, Colombia, in 2000 and 2005 respectively. He attended Purdue University, Indiana U.S.A. for his Ph.D. program where he worked at the Purdue Robot Vision Lab, however, he switched to

Marquette University in 2019 and is expecting his PhD degree for 2022 from the COVISS Lab. Currently, he is a tenured professor at the school of Electrical, Electronics, Physics, and Computer Science at Universidad Tecnológica de Pereira, UTP, in Pereira, Colombia. His major fields of work and research are

Computer Vision, Image Understanding, Deep Convolutional Neural Networks, Precision Agriculture, and Industrial Automation. He was awarded the Fulbright Scholarship in 2006.

ORCID: <https://orcid.org/0000-0001-7760-5874>



Carlos Alberto Ramírez-Vanegas received the bachelor's degree and master's degrees in electrical engineering from the Technological University of Pereira, Pereira, Colombia, in 2012 and 2018, respectively. He has worked as a professor in the mathematics department of the

Technological University of Pereira since 2014. His research interests include numerical analysis, optimal control and optimization techniques.

ORCID: <https://orcid.org/0000-0002-6646-4209>